Applied Mathematics Letters 107 (2020) 106487

Contents lists available at ScienceDirect

Applied Mathematics Letters

www.elsevier.com/locate/aml

Shape transformation using the modified Allen–Cahn equation

Hyundong Kim [a], Sungha Yoon [a], Jian Wang [b], Chaeyoung Lee [a], Sangkwon Kim [a], Jintae Park [a], Junseok Kim [a,*]

[a] *Department of Mathematics, Korea University, Seoul 02841, Republic of Korea*
[b] *School of Mathematics and Statistics, Nanjing University of Information Science and Technology, Nanjing, 210044, China*

ARTICLE INFO

Article history:
Received 10 March 2020
Received in revised form 14 May 2020
Accepted 14 May 2020
Available online 17 May 2020

Keywords:
Phase-field
Allen–Cahn equation
Shape transformation
Metamorphosis

ABSTRACT

In this paper, we propose a phase-field model for the shape transformation and its simple numerical method. The proposed phase-field model is based on the Allen–Cahn equation, which is a second-order nonlinear parabolic partial differential equation and originally arises from modeling phase separation in alloys. The numerical scheme is a hybrid method using the operator splitting method. To validate the proposed phase-field model for the shape transformation, we perform two- and three-dimensional shape metamorphosis. The proposed phase-field model is also compared with the linear interpolation. The computational results demonstrate that the proposed mathematical model satisfactorily and naturally simulate the shape transformation.

1. Introduction

Shape transformation has many applications in various fields such as remote sensing technique, medicine, graphic technique, and special effects creation [1,2]. Shape transformation can be performed between objects of two- and three-dimensional shapes. In the related previous work [3], metamorphosis of solid models represented as k level-set in a set of surface points $\mathcal{S} = \{\mathbf{x} : \phi(\mathbf{x}, t) = k\}$, which is governed by the following partial differential equation:

$$\phi_t(\mathbf{x}, t) = |\nabla\phi(\mathbf{x}, t)|\tau(\mathbf{x}, t),$$

where τ is the signed distance transform. In order to do three-dimensional (3D) morphing, the authors in [4] used the strain field interpolation. Linear strain interpolation is used for producing morphing results to avoid oscillations in local size over time. However, this method gives uneven rates of shape change overtime in cases of very large deformations. To overcome it, the authors proposed modified strain interpolation which

* Corresponding author.
E-mail addresses: rlagusehd@korea.ac.kr (H. Kim), cfdkim@korea.ac.kr (J. Kim).
URL: http://math.korea.ac.kr/∼cfdkim/ (J. Kim).

https://doi.org/10.1016/j.aml.2020.106487
0893-9659/

is to force the lengths of edges parallel to the coordinate axes to change linearly with time because the strain field arises due to length changes of line segments. The authors in [5] proposed a mathematically well-defined method and a Eulerian approach was constructed for mapping surfaces with different topologies. This work was mainly to find the implicit functions for the input meshes, and the zero level sets were visualized with the marching cube algorithm, then interpolated the functions with a morphing technique. By finding the velocity field that tracks the zero level sets, at last they detected the singular areas and removed them. The authors in [6] proposed four shape morphing methods using an elliptic partial differential equation (PDE). They adapted the Bloor–Wilsons PDE method originally introduced by Bloor and Wilson to generate free-form surfaces [7]. It expressed the solution of a given PDE in terms of a Fourier series. In addition, extensive researches on shape transformation or morphing were performed, using variational implicit functions [8], Poisson equation-based interpolation [9] and object-space morphing [10]. The main purpose of this study is to propose a phase-field model for shape transformation and its simple numerical scheme. The major advantages of the proposed phase-field model are its simplicity and ability to simulate naturally shape transformation.

The paper is organized in the following manner. In Section 2, we describe the governing equation and numerical solution algorithm. To simulate the shape transformation, we perform the numerical experiments using the proposed phase-field model in Section 3. In Section 4, conclusions are given.

2. Governing equation and numerical solution algorithm

2.1. Governing equation

We propose the modified Allen–Cahn (mAC) equation for the morphological transformation as follows:

$$\frac{\partial \phi(\mathbf{x},t)}{\partial t} = -\frac{F'(\phi(\mathbf{x},t))}{\epsilon^2} + \Delta\phi(\mathbf{x},t) + \alpha\sqrt{F(\phi(\mathbf{x},t))}(\psi(\mathbf{x}) - \phi(\mathbf{x},t)), \tag{1}$$

where $\mathbf{x} \in \Omega,\ t > 0$, $\phi(\mathbf{x},t)$ is the phase-field, ϵ is an interfacial transition layer related parameter, α is a fidelity parameter, and $F(\phi) = 0.25(\phi^2-1)^2$ is a double-well potential. We set the source shape by $\phi(\mathbf{x},0)$ and the target shape by $\psi(\mathbf{x})$. Here, we assume $\min_{\mathbf{x}\in\Omega}\psi(\mathbf{x}) = -1$ and $\max_{\mathbf{x}\in\Omega}\psi(\mathbf{x}) = 1$ because of the choice of the double-well potential. Otherwise, we redefine the target as

$$\psi(\mathbf{x}) := \frac{2\psi(\mathbf{x}) - \max_{\mathbf{x}\in\Omega}\psi(\mathbf{x}) - \min_{\mathbf{x}\in\Omega}\psi(\mathbf{x})}{\max_{\mathbf{x}\in\Omega}\psi(\mathbf{x}) - \min_{\mathbf{x}\in\Omega}\psi(\mathbf{x})}. \tag{2}$$

We can also derive Eq. (1) using the gradient flow in L^2 of the Liapunov energy functional [11]:

$$\mathcal{E}(\phi) := \int_\Omega \left[\frac{F(\phi)}{\epsilon^2} + \frac{1}{2}|\nabla\phi|^2 + \frac{\alpha}{2}\left(\left(\frac{\phi^3}{3} - \phi\right)\psi - F(\phi)\right)\right] d\mathbf{x}. \tag{3}$$

By taking the variational derivative of Eq. (3) in the $L^2(\Omega)$ space, we obtain Eq. (1) from $\partial\phi/\partial t = -\delta\mathcal{E}/\delta\phi$. Furthermore, we have energy dissipative law, $d\mathcal{E}/dt = -\int_\Omega (\partial\phi/\partial t)^2\, d\mathbf{x}$. The basic mechanism of the proposed phase-field model will be described in detail in Section 3.1. Substituting $\alpha = 0$ in Eq. (1) gives the classical AC equation [12,13] which describes the process of phase separation in a binary alloy. In [14], the authors proposed a modified AC equation with a different source term for the piecewise constant Mumford–Shah functional for image segmentation.

2.2. Numerical solution algorithm

First, we discretize Eq. (1) in three-dimensional space $\Omega = (a, b) \times (c, d) \times (e, f)$. Let $\Omega = \{(x_i, y_j, z_k) : x_i = a + h(i - 0.5), y_j = c + h(j - 0.5), z_k = e + h(k - 0.5), 1 \le i \le N_x, 1 \le j \le N_y, 1 \le k \le N_z\}$ be the cell-centered discrete domain, where N_x, N_y, and N_z are the number of spatial points, $h = (b-a)/(N_x-1) = (d - c)/(N_y - 1) = (e - f)/(N_z - 1)$ is the uniform grid size. Let $\phi^n_{ijk} = \phi(x_i, y_j, z_k, n\Delta t)$, where Δt is the temporal step size. Applying the operator splitting method to split Eq. (1) into the diffusion, reaction, and fidelity term:

$$\frac{\partial \phi(\mathbf{x}, t)}{\partial t} = \Delta \phi(\mathbf{x}, t), \tag{4}$$

$$\frac{\partial \phi(\mathbf{x}, t)}{\partial t} = -\frac{F(\phi(\mathbf{x}, t))}{\epsilon^2}, \tag{5}$$

$$\frac{\partial \phi(\mathbf{x}, t)}{\partial t} = \alpha\sqrt{F(\phi(\mathbf{x}, t))}(\psi(\mathbf{x}) - \phi(\mathbf{x}, t)). \tag{6}$$

Then, the numerical solution of the governing equation (1) can be found in the following three steps. As the first step, the diffusion term (4) is solved by the explicit Euler method

$$\frac{\phi^*_{ijk} - \phi^n_{ijk}}{\Delta t} = \Delta_d \phi^n_{ijk}, \tag{7}$$

where $\Delta_d \phi^n_{ijk} = (\phi^n_{i+1,j,k} + \phi^n_{i-1,j,k} + \phi^n_{i,j+1,k} + \phi^n_{i,j-1,k} + \phi^n_{i,j,k+1} + \phi^n_{i,j,k-1} - 6\phi^n_{ijk})/h^2$. As the second step, the reaction term (5) is solved using the closed-form solution obtained from separation of variables

$$\phi^{**}_{ijk} = \phi^*_{ijk} \Big/ \sqrt{\left(1 - \left(\phi^*_{ijk}\right)^2\right) e^{-\frac{2\Delta t}{\epsilon^2}} + \left(\phi^*_{ijk}\right)^2}. \tag{8}$$

These two steps consist of the explicit hybrid numerical scheme for the AC equation [15]. Finally, we use the fully implicit Euler method for the fidelity term (6)

$$\frac{\phi^{n+1}_{ijk} - \phi^{**}_{ijk}}{\Delta t} = \alpha\sqrt{F\left(\phi^{**}_{ijk}\right)}(\psi_{ijk} - \phi^{n+1}_{ijk}). \tag{9}$$

From Eq. (9), we get

$$\phi^{n+1}_{ijk} = \left(\phi^{**}_{ijk} + \Delta t\alpha\psi_{ijk}\sqrt{F\left(\phi^{**}_{ijk}\right)}\right) \Big/ \left(1 + \Delta t\alpha\sqrt{F\left(\phi^{**}_{ijk}\right)}\right). \tag{10}$$

Let $\|\phi^n\|_\infty = \max_{i,j,k} |\phi^n_{ijk}|$ for $n = 0, 1, 2, \ldots$ be the discrete l_∞-norm.

Theorem 1. *If $\|\phi^0\|_\infty \le 1$, then the proposed numerical scheme (7), (8), (10) has a time step constraint for stability as $\Delta t \le h^2/6$ and $\|\phi^{n+1}\|_\infty \le 1$ for all $n \ge 0$.*

Proof. Without loss of generality, let $\|\phi^n\|_\infty \le 1$ for some n. By using the discrete von Neumann stability analysis, the stability condition for the first step, Eq. (7), is $\Delta t \le h^2/(2d)$, where d is the dimension of the computational space [16]. Therefore, for the three-dimensional case, the stability constraint for the time step is $\Delta t \le h^2/6$. For the second step, Eq. (8), it is unconditionally stable and $|\phi^{**}_{ijk}|$ is bounded by 1 if $|\phi^*_{ijk}| \le 1$, which is satisfied because of the discrete maximal principle for the diffusion equation. For the third step, Eq. (10), it is unconditionally stable and $|\phi^{n+1}_{ijk}|$ is bounded by 1 if $|\phi^{**}_{ijk}| \le 1$, i.e.,

$$|\phi^{n+1}_{ijk}| \le \frac{|\phi^{**}_{ijk}| + \Delta t\alpha|\psi_{ijk}|\sqrt{F\left(\phi^{**}_{ijk}\right)}}{1 + \Delta t\alpha\sqrt{F\left(\phi^{**}_{ijk}\right)}} \le \frac{1 + \Delta t\alpha\sqrt{F\left(\phi^{**}_{ijk}\right)}}{1 + \Delta t\alpha\sqrt{F\left(\phi^{**}_{ijk}\right)}} = 1, \tag{11}$$

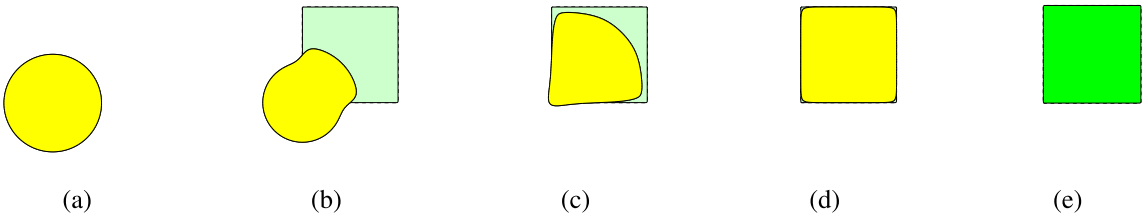

Fig. 1. (a) and (e) are the source and target shapes, respectively. (b)–(d) are the snapshots of $\phi(x, y, t)$ at $t = 20\Delta t$, $100\Delta t$, and $320\Delta t$, respectively.

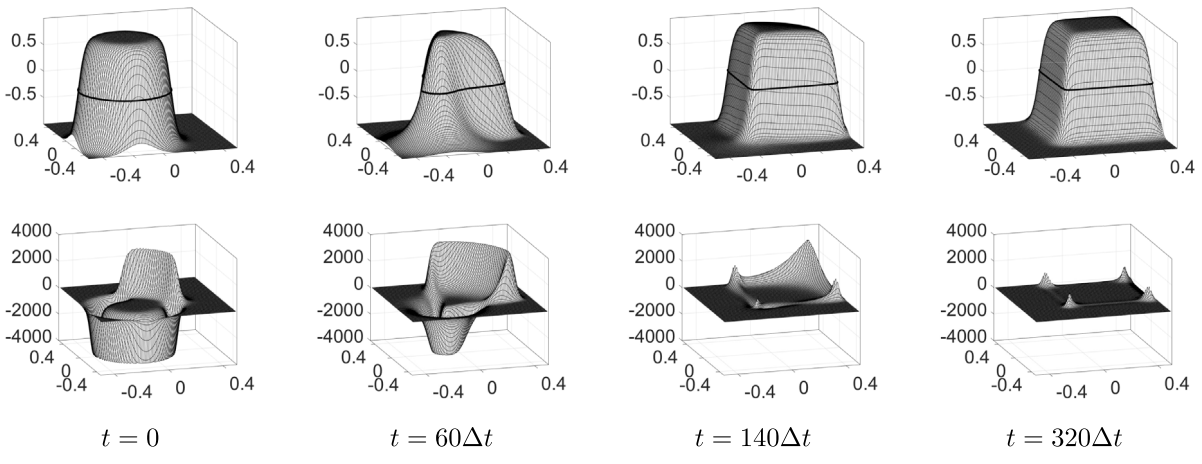

Fig. 2. Snapshots of the mesh plots of transforming shape and the evolving fidelity term over time in the first and second rows, respectively. In the first row, solid line is the zero level set of ϕ.

where we have used Eq. (2), $|\psi_{ijk}| \leq 1$. Therefore, the overall time step constraint is $\Delta t \leq h^2/6$ and $\|\phi^{n+1}\|_\infty \leq 1$ for all $n \geq 0$. □

3. Numerical experiments

3.1. Basic mechanism of the proposed phase-field model

First, we describe the basic mechanism of the proposed phase-field model using a simple example in the two-dimensional (2D) domain, $\Omega = (-0.5, 0.5)^2$. Let $\phi(x, y, 0)$ and $\psi(x, y)$ be the source (Fig. 1(a)) and target (Fig. 1(e)) shapes:

$$\phi(x, y, 0) = \tanh\left(\frac{0.3 - \sqrt{(x + 0.15)^2 + (y + 0.15)^2}}{\sqrt{2}\epsilon}\right),$$
$$\psi(x, y) = \tanh\left(\frac{-\sqrt{\max(x^*, 0)^2 + \max(y^*, 0)^2} - \min(\max(x^*, y^*), 0)}{\sqrt{2}\epsilon}\right),$$

where $\epsilon = 0.03$, $x^* = |x - 0.15| - 0.3$, and $y^* = |y - 0.15| - 0.3$. The process of transforming the source to target shapes over time is shown in Fig. 1. Here, $N_x = N_y = 100$, $h = 0.01$, $\Delta t = 0.15h^2$, and $\alpha = 6000$ are used.

The first and second rows in Fig. 2 show the mesh plots of transforming ϕ and the evolution of the fidelity term $\alpha\sqrt{F\left(\phi^{**}_{ijk}\right)}(\psi_{ijk} - \phi^{n+1}_{ijk})$ over time, respectively. At $t = 320\Delta t$, the value of fidelity term is

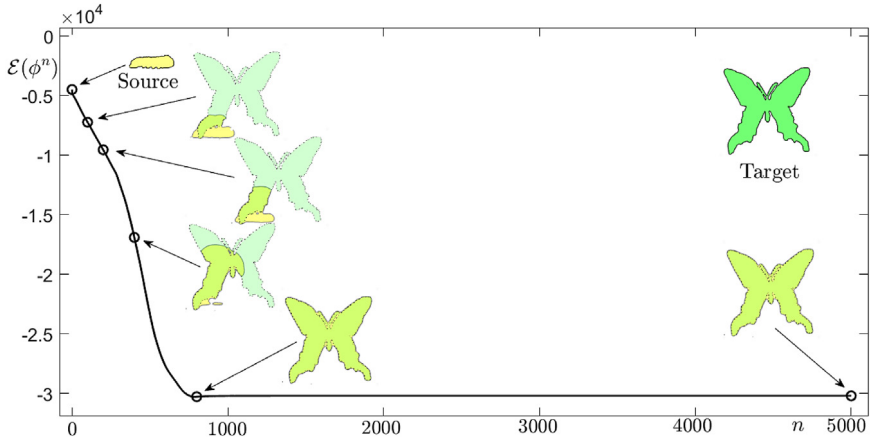

Fig. 3. Temporal evolution of the total energy $\mathcal{E}(\phi^n)$.

Table 1
Errors and rates of convergence for ϕ. Note that the size of time step is $\Delta t = 0.025h^2$.

$(h,\ h/2)$	(1/16, 1/32)	Rate	(1/32, 1/64)	Rate	(1/64, 1/128)	Rate	(1/128, 1/256)
$\left\|e^{\Delta t,h}\right\|_2$	0.1279	1.994	0.0321	2.032	0.0078	2.003	0.0019

almost zero except the corner regions of the square, which implies that transformation approaches a steady state. Therefore, the basic mechanism of the proposed phase-field model is as follows: The AC equation part preserves smooth phase transition layer. Meanwhile, the fidelity term adds the phase-field value toward target position and subtracts the phase-field value outside the target position.

3.2. Convergence test

We conduct a convergence test to show that the proposed scheme is first-order accurate in time and second-order accurate in space. We use the same initial condition and parameters used in Section 3.1 except for mesh size and time step size. Let $\left\|e^{\Delta t,h}\right\|_2 = \sqrt{\sum_{i,j}\left(e_{ij}^{\Delta t,h}\right)^2 / \left(N_x^{\Delta t,h} N_y^{\Delta t,h}\right)}$ be the discrete l_2-norm of relative error, where $e_{ij}^{\Delta t,h}$ is an error between coarse and fine values defined as $e_{ij}^{\Delta t,h} = \left|\phi_{ij}^{\Delta t,h} - 0.25\left(\phi_{2i-1,2j-1}^{\Delta t/4,h/2} + \phi_{2i-1,2j}^{\Delta t/4,h/2} + \phi_{2i,2j-1}^{\Delta t/4,h/2} + \phi_{2i,2j}^{\Delta t/4,h/2}\right)\right|$. The rate of convergence is defined by $\log_2\left(\left\|e^{\Delta t,h}\right\|_2 / \left\|e^{\Delta t/4,h/2}\right\|_2\right)$. Table 1 shows the result of rate of convergence at $t \approx 0.0001$, which shows that the proposed numerical method is temporally first-order and spatially second-order. Note that we can use high-order temporal schemes. However, in this study, we focus on a simple and robust scheme.

3.3. Shape transformation in two-dimensional space

Let us consider a more complex example which is image transformation from a larva shape source into a butterfly shape target using the proposed phase-field model. Fig. 3 depicts a transformation from the larva to butterfly shapes at the indicated times with temporal evolution of the total energy $\mathcal{E}(\phi^n)$. According to the result, the total energy is non-increasing. Here, $h = 1/356$, $\Delta t = 0.15h^2$, $\epsilon = 4h$, and $\alpha = 10^5$ are used.

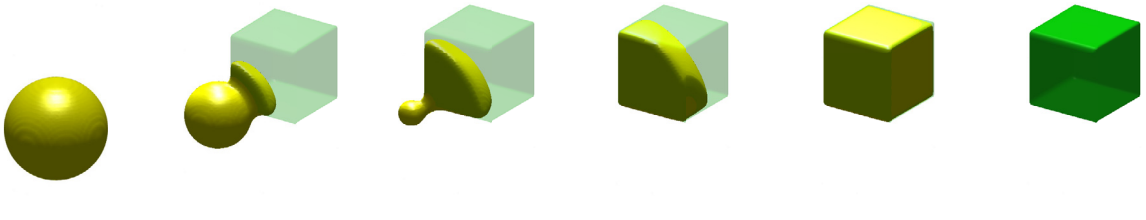

Fig. 4. (a) and (f) are the source and target shapes, respectively. (b)–(e) are the snapshots of $\phi(x, y, z, t)$ at $t = 8\Delta t$, $20\Delta t$, $34\Delta t$, and $70\Delta t$, respectively.

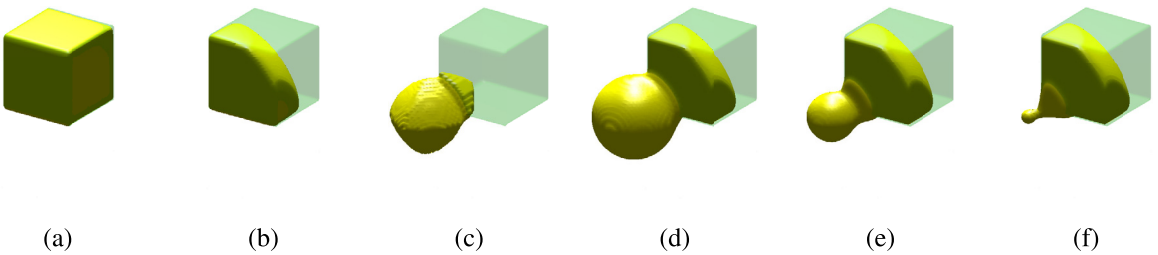

Fig. 5. (a), (b), and (c) are snapshots of shape transformation at $t = 34\Delta t$ with $\epsilon = h$, $\epsilon = 0.5h$, and $\epsilon = 0.25h$, respectively. (d), (e), and (f) are snapshots of deformation at $t = 34\Delta t$ with $K = 0.05$, $K = 0.25$, and $K = 0.5$, respectively.

3.4. Shape transformation in three-dimensional space

3.4.1. Effect of ϵ and α

Next, we study the effect of parameter ϵ on the shape transformation dynamics. We consider a sphere of radius 0.6 with center at $(-0.3, -0.3, -0.3)$ as a source shape and a unit cube with center $(0.3, 0.3, 0.3)$ as a target shape in domain $\Omega = (-1, 1)^3$ with $N_x = N_y = N_z = 64$ as shown in Fig. 4(a) and (f), respectively. Fig. 4(b)–(e) show snapshots of shape transformation from sphere to cube with $\Delta t = 0.15h^2$, $\epsilon = 0.5h$, and $\alpha = 25000$.

Now, we change the parameter ϵ by doubling or halving it and repeat the previous test with the same conditions. Fig. 5(a), (b) and (c) show snapshots of transformation at the same time $t = 34\Delta t$ with $\epsilon = h$, $\epsilon = 0.5h$, and $\epsilon = 0.25h$, respectively. We can see that speed of transformation is fast when ϵ becomes larger. Conversely, when ϵ becomes smaller, the rate of change is slow and the shape is not smooth.

Next, we investigate the effect of α on the shape transformation dynamics. We generalize α to control the speed of the dissolution and the growth. We define the fidelity parameter as $\alpha(\psi) = \lambda\psi$ if $\psi > 0$; otherwise $\alpha(\psi) = -\lambda K\psi$, where K is a scaling factor and $\lambda = 25000$. Fig. 5(d), (e), and (f) show snapshots of deformation at $t = 34\Delta t$ with different values of $K = 0.05$, 0.25, and 0.5, respectively. The fidelity parameter $\alpha(\psi)$ controls the speed of deformation.

3.4.2. Complex shape case

Finally, we consider more complex 3D shapes such as Stanford Bunny (Fig. 6(a) and (g)) and Stanford Armadillo (Fig. 6(f) and (l)) for the source and target shapes, respectively. We set $N_x = N_y = N_z = 200$, $h = 0.005$, $\Delta t = 0.15h^2$, $\epsilon = 0.5h$, and $\alpha = 5 \times 10^5$. Fig. 6(b)–(e) show snapshots of shape transformation from Bunny to Armadillo using the proposed phase-field model.

We present a linear interpolation result for comparison.

$$\phi_L(x, y, z, \theta) = (1 - \theta)\,\phi(x, y, z, 0) + \theta\psi(x, y, z), \quad \text{for } 0 \le \theta \le 1.$$

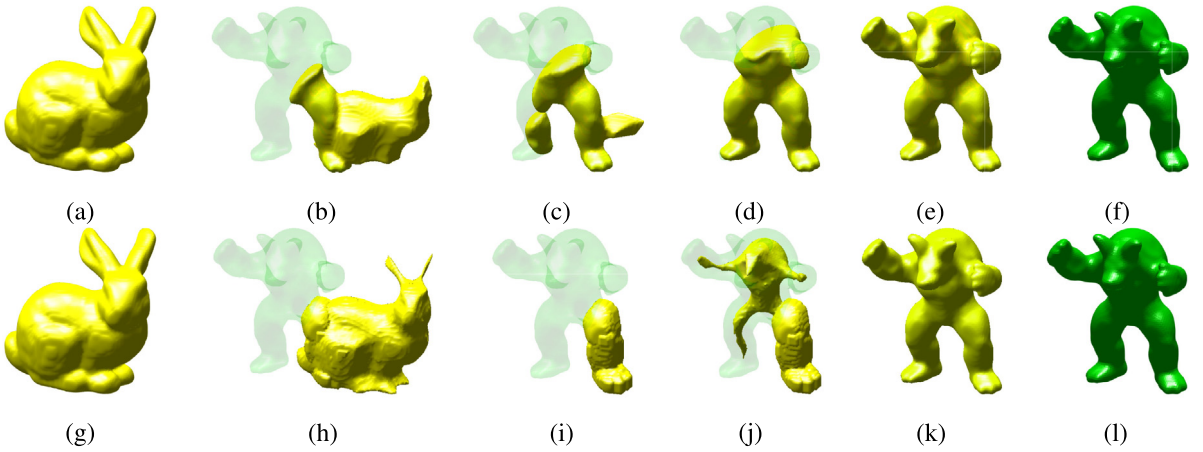

Fig. 6. (a) and (f) are the source and target shapes, respectively. (b)–(e) are the snapshots of $\phi(x, y, z, t)$ at $t = 20\Delta t$, $40\Delta t$, $60\Delta t$, and $150\Delta t$, respectively. (g) and (l) are the source and target shapes, respectively. (h)–(k) are the snapshots of $\phi_L(x, y, z, \theta)$ at $\theta = 0.49999$, 0.5, 0.50001, and 1, respectively.

For increasing θ values, Fig. 6(h)–(k) show snapshots of shape transformation from Bunny to Armadillo using the linear interpolation. As shown in the top row in Fig. 6, the shape structure changes continuously and smoothly when the proposed phase-field model is used. The bottom row in Fig. 6 demonstrates the sudden and unnatural morphological deformation that scope out of our intuition.

4. Conclusions

In this article, we proposed the modified Allen–Cahn equation for the shape transformation and its simple numerical method. The numerical scheme is explicit, therefore, its implementation is easy and it does not have any domain size restriction. To validate the proposed phase-field model for the shape transformation, we performed two- and three-dimensional shape metamorphosis. The numerical results demonstrated that the proposed mathematical model satisfactorily and naturally simulate the shape transformation. An interesting future work will be developing a much more faster algorithm.

CRediT authorship contribution statement

Hyundong Kim: Conceptualization, Methodology, Software, Validation, Formal analysis, Investigation, Data curation, Writing - original draft, Writing - review & editing, Visualization, Project administration. **Sungha Yoon:** Software, Validation, Investigation, Writing - original draft, Writing - review & editing, Visualization. **Jian Wang:** Software, Investigation, Writing - original draft. **Chaeyoung Lee:** Investigation, Validation, Writing - original draft. **Sangkwon Kim:** Validation, Investigation, Writing - original draft. **Jintae Park:** Software, Investigation, Writing - original draft. **Junseok Kim:** Conceptualization, Methodology, Software, Validation, Investigation, Formal analysis, Writing - original draft, Writing - review & editing, Visualization, Supervision, Project administration, Funding acquisition.

Acknowledgments

The corresponding author (J. Kim) was supported by Basic Science Research Program through the National Research Foundation of Korea (NRF) funded by the Ministry of Education, South Korea (NRF-2019R1A2C1003053).

References

[1] S.Y. Lee, K.Y. Chwa, J. Hahn, S.Y. Shin, Image morphing using deformation techniques, J. Vis. Comput. Animat. 7 (1) (1996) 3–23.
[2] M. Steyvers, Morphing techniques for manipulating face images, Behav. Res. Methods Instrum. Comput. 31 (2) (1999) 359–369.
[3] D.E. Breen, R.T. Whitaker, A level-set approach for the metamorphosis of solid models, IEEE Trans. Vis. Comput. Graphics 7 (2) (2001) 173–192.
[4] H.B. Yan, S.M. Hu, R.R. Martin, 3D morphing using strain field interpolation, J. Comput. Sci. Technol. 22 (1) (2007) 147–155.
[5] H. Park, Y. Cho, S. Bang, S.H. Lee, An Eulerian approach for constructing a map between surfaces with different topologies, Comput. Graph. Forum 35 (7) (2016) 11–19.
[6] G. Gonzalez Castro, H. Ugail, Shape morphing of complex geometries using partial differential equations, J. Multimed. 2 (6) (2007) 15–25.
[7] M.I. Bloor, M.J. Wilson, Using partial differential equations to generate free-form surfaces, Comput. Aided Des. 22 (4) (1990) 202–212.
[8] G. Turk, J.F. O'brien, Shape transformation using variational implicit functions, in: ACM SIGGRAPH 2005 Courses, 2005, 13-es.
[9] D. Xu, H. Zhang, Q. Wang, H. Bao, Poisson shape interpolation, Graph. Models 68 (3) (2006) 268–281.
[10] M. Alexa, D. Cohen-Or, D. Levin, As-rigid-as-possible shape interpolation, in: Proceedings of the 27th Annual Conference on Computer Graphics and Interactive Techniques, 2000, pp. 157–164.
[11] F. Lin, X. He, X. Wen, Fast, unconditionally energy stable large time stepping method for a new Allen–Cahn type square phase-field crystal model, Appl. Math. Lett. 98 (2019) 248–255.
[12] S.M. Allen, J.W. Cahn, A microscopic theory for antiphase boundary motion and its application to antiphase domain coarsening, Acta Mater. 27 (6) (1979) 1085–1095.
[13] J. Niu, M. Xu, G. Yao, An efficient reproducing kernel method for solving the Allen–Cahn equation, Appl. Math. Lett. 89 (2019) 78–84.
[14] Y. Li, J. Kim, An unconditionally stable hybrid method for image segmentation, Appl. Numer. Math. 82 (2014) 32–43.
[15] D. Jeong, J. Kim, An explicit hybrid finite difference scheme for the Allen–Cahn equation, J. Comput. Appl. Math. 340 (2018) 247–255.
[16] J.W. Thomas, Numerical Partial Differential Equations: Finite Difference Methods, Springer Science & Business Media, New York, 2013.